A New Method to Analyse the Role of Surface Plasmon Polaritons on Dielectric-Metal Interfaces

Ricardo A. Marques Lameirinhas, João Paulo N. Torres, António Baptista, and Maria João Marques Martins

***Abstract*—At nano-scale new phenomena have been discovered, allowing devices' miniaturisation, energy harvesting, and power reduction. The Extraordinary Optical Transmission (EOT) phenomenon was reported in 1998 by Ebessen, who stated that the resonant peaks in the response of metallic nano antennas were more intense than predicted by classical diffraction theories. Years later, the main reason for this behaviour was attributed to the Surface Plasmon Polaritons (SPP), at least in ultraviolet and visible regions. In this article, a new method to model the radiation-matter interaction on a dielectric-metal interface is proposed, based on Maxwell's equations and Fresnel Coefficients in absorbing media. Transmission percentage, angle and propagation length are obtained for a rigorous sweep on incident angle and wavelength. The results taken using some noble metals allow us to observe the presence of surface phenomena at expected SPP resonances. First, it is noticeable huge values of transmission in ultraviolet and visible regions, meaning that the metal does not reflect all the radiation. Also, the transmission angle tends to be higher, meaning huge surface components. Furthermore, the transmission length is on orders of 50-100 nm, meaning that phenomena as EOT only occurs at the nano-scale, since waves should arrive at another interface before being absorbed.**

***Index Terms*—Extraordinary optical transmission, light patterns, nano antennas, optical devices, subwavelength structures, surface plasmon polaritons.**

I. Introduction

THE interest in nanotechnology has been increasing in the last decades, not only due to the foreseeable advantages of nano-sized devices but also because new phenomena were discovered. Thus, it is crucial to increase our knowledge about light-matter interaction and how to manipulate light to obtain certain regimes or phenomena that allow the development of novel devices at nano-scale [1]–[5]. One excellent example is the Extraordinary Optical Transmission (EOT), an effect that is only visible at optical frequencies on nano-structures. The light-matter interaction knowledge is then the key to designing miniaturised and low-power devices [1]–[7].

In 1998, Ebbesen reported unusual transmission peaks at metallic nano arrays [1]. The optical response of these structures has higher transmission in certain wavelengths than expected by classical diffraction theories, or in other words, the light intensity on the target is higher than the predictable. For that reason, the phenomenon is known as Extraordinary Optical Transmission. Ebbesen associated this phenomenon with Surface Plasmon Polaritons (SPP), which are the result of a strong coupling between incident light and plasmons (electronic excitations) on the surface [1]–[4], [8], [9].

Since that, several authors focus their research not only on Surface Plasmon Polaritons, but also on the possible applications of EOT in novel photonic and optoelectronic devices in several fields such as energy, medicine, information, defence or environment [1], [5]–[7].

In this article, dielectric-metal interfaces are analysed using a new approach. It starts with the way materials must be characterised, specially at nano-sized devices, followed by a brief explanation of SPP behaviour. The novel and implemented method is described and analysed. The obtained results are presented, corroborating the idea that SPP are the main agents of EOT in the ultraviolet and visible spectral regions. The wavevector behaviour (representative of a light wave, ray, or particle) is presented and analysed as function of incident angle and wavelength for four different metals (gold, silver, aluminium, and copper) with different resonance frequencies. Both method and theoretical approach are based on Maxwell's equations, allowing the validation of the proposed methodology.

II. Methodology

A. Material Characterisation

Light-metal interaction might be characterised mainly due to the movement of the free electrons in the metal.

According to Drude's model, the oscillations of those electrons and of the electric field are in phase opposition. Consequently, most of the metals have a negative electrical permittivity leading to their high reflection coefficient [6].

Most metals may support some interesting phenomena, such as the propagation of SPP. Surface Plasmon are oscillations of the metals' free electrons that can couple with the incident radiation, leading to SPP [6], [8], [9].

Manuscript received May 3, 2022; revised June 6, 2022; accepted June 7, 2022. Date of publication June 13, 2022; date of current version June 22, 2022. This work was supported in part by FCT/MCTES through national funds and in part by cofounded EU funds under Project UIDB/50008/2020, and in part by FCT the research under Grant UI/BD/151091/2021. *(Corresponding author: Ricardo A. Marques Lameirinhas.)*

Ricardo A. Marques Lameirinhas is with the Instituto Superior Técnico, 1049-001 Lisboa, Portugal, and also with the Instituto de Telecomunicações, 3810-193 Lisboa, Portugal (e-mail: ricardo.lameirinhas@tecnico.ulisboa.pt).

João Paulo N. Torres is with the Instituto de Telecomunicações, 3810-193 Lisboa, Portugal, and also with the Academia Militar/CINAMIL, 1169-203 Amadora, Portugal (e-mail: joaoptorres@hotmail.com).

António Baptista is with the Instituto Superior Técnico, 1049-001 Lisboa, Portugal (e-mail: baptista@tecnico.ulisboa.pt).

Maria João Marques Martins is with the Academia Militar/CINAMIL, 1169-203 Amadora, Portugal (e-mail: mariajoaomartins2@gmail.com).

Digital Object Identifier 10.1109/JPHOT.2022.3181967

Thus, these phenomena are especially dependent on the metals' electrical behaviour at different frequencies. For this reason, the metals' models should be adapted for the optical frequencies and for nano-scale structures.

The first approach to modelling the materials' optical properties is based on the electron movement equation, which describes the movement of free electrons in the metal and consequently the generated electrical current for the incident radiation. This equation is presented on Expression (1), for a direction vector r where $\bar{\boldsymbol{E}}_{\mathbf{0}}$ is the sinusoidal amplitude of the incident electrical field with angular frequency ω, q and m_e are respectively the electron's modulus of charge and its effective mass and Γ is the damping factor that is related to the electrons' Fermi velocity v_F and average propagation distance l by $\Gamma = v_F/l$. This factor relates the energy loss due to electrons collisions [6], [10].

From Expression (1) is possible to obtain the relative electrical permittivity, which is presented on Expression (2). In this expression ω_p is the plasma frequency, which is electrically described as $\omega_p = \sqrt{\tilde{n}q^2/(m_e\epsilon_0)}$ where $\tilde{n}$ is the free electrons density and ϵ_0 the vacuum electrical permittivity [6], [10].

$$m_e\frac{\partial^2 \boldsymbol{r}}{\partial t^2} + m_e\Gamma\frac{\partial \boldsymbol{r}}{\partial t} = q\bar{\boldsymbol{E}}_{\mathbf{0}} \tag{1}$$

$$\bar{\epsilon}_{Drude}(\omega) = 1 - \frac{\omega_p^2}{\omega^2+\Gamma^2} + j\frac{\Gamma\omega_p^2}{\omega(\omega^2+\Gamma^2)} \tag{2}$$

This model is sufficient to characterise metals behaviour at frequencies in the infrared region and below it.

In the near-infrared and visible regions other models should be obtained, namely due to correction regarding the influence of bound electrons due to intraband transitions.

Expression (3) describes the movement of bound electrons, where γ is the radiation damping factor for the case of bound electrons, α is the potential force restitution coefficient and m is the bound electrons' effective mass.

Based on Expression (3) it is possible to establish the contribution of bound electrons to the relative electrical permittivity, presented in Expression (4) [6], [10]. In this case, $\tilde{\omega} = \sqrt{\tilde{\tilde{n}}q^2/(m\epsilon_0)}$ and $\omega_i = \sqrt{\alpha/m}$ for $\tilde{\tilde{n}}$ bound electrons density.

$$m\frac{\partial^2 \boldsymbol{r}}{\partial t^2} + m\gamma\frac{\partial \boldsymbol{r}}{\partial t} + \alpha\boldsymbol{r} = q\bar{\boldsymbol{E}}_{\mathbf{0}} \tag{3}$$

$$\bar{\epsilon}_{be}(\omega) = 1 + \frac{\tilde{\omega}_p^2(\omega_i^2-\omega^2)}{(\omega_i^2-\omega^2)^2+\gamma^2\omega^2} + j\frac{\gamma\tilde{\omega}_p^2\omega}{(\omega_i^2-\omega^2)^2+\gamma^2\omega^2} \tag{4}$$

Thus, it is possible to consider that the relative dielectric function results from the sum of different contributions regarding free and bound electrons, leading to more precise models. This is the base of the Drude-Lorentz model, in which the permittivity function is presented on Expression (5) [6], [7], [10], [12].

$$\bar{\epsilon}(\omega) = 1 - \frac{\Omega_p^2}{\omega(\omega+j\Gamma_0)} + \sum_{n=1}^{N}\frac{f_n\omega_p^2}{(\omega_n^2-\omega^2)-j\omega\Gamma_n} \tag{5}$$

The most used metals are Gold, Silver, Aluminium and Copper due to their optical properties that are analysed in the following sections. In table I are presented the constant values for these metals, according to models and fitting made by Rakic *et al.* [11], [12]. Here, the plasma angular frequency ω_p is given by ω_0 and $\Omega_p = f_0^{1/2}\omega_p$.

TABLE I
RAKIC'S DRUDE-LORENTZ PARAMETERS

	Gold			Silver		
n	f_n	$\omega_n\,[eV]$	$\Gamma_n\,[eV]$	f_n	$\omega_n\,[eV]$	$\Gamma_n\,[eV]$
0	0.760	9.030	0.053	0.845	9.010	0.048
1	0.024	0.415	0.241	0.065	0.816	3.886
2	0.010	0.830	0.345	0.124	4.481	0.452
3	0.071	2.969	0.870	0.011	8.185	0.065
4	0.601	4.304	2.494	0.840	9.083	0.840
5	4.384	2.214	13.32	5.646	20.290	2.419

	Aluminium			Copper		
n	f_n	$\omega_n\,[eV]$	$\Gamma_n\,[eV]$	f_n	$\omega_n\,[eV]$	$\Gamma_n\,[eV]$
0	0.523	14.98	0.047	0.575	10.830	0.030
1	0.227	0.162	0.333	0.061	0.291	0.378
2	0.050	1.544	0.312	0.104	2.957	1.056
3	0.166	1.808	1.351	0.723	5.300	3.213
4	0.030	3.473	3.382	0.638	11.180	4.305
5	-	-	-	-	-	-

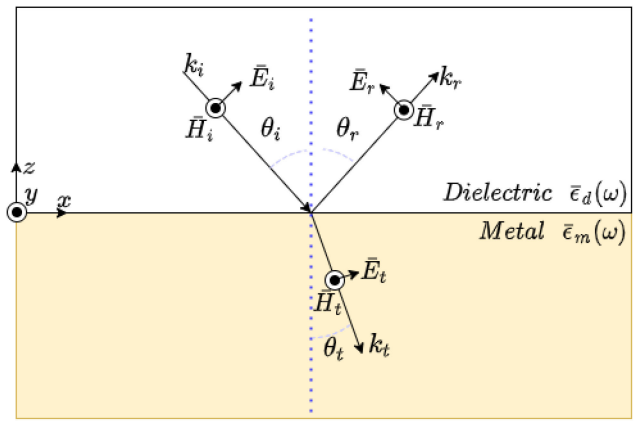

Fig. 1. Dielectric-metal interface (TM wave representation).

B. Surface Plasmon Polaritons Analysis

A plasmon, which is considered a quasiparticle, is a quantum of a plasma oscillation (redistribution of plasma's free electrons), just as light is the optical oscillation of photons. Therefore, plasmons are collective oscillations that can be coupled with photons, creating another quasiparticle called (plasmon) polariton. So, a surface plasmon and a surface plasmon polariton are not the same, even though they have a straight relation [6]–[8], [10].

Then, SPP are electromagnetic waves, propagating at the interface, between a metal/plasma and a dielectric. A TM wave is represented on Fig. 1 at a dielectric-metal interface. Both media are non-magnetic and semi-unlimited. The TM wave is described by a wavevector $\bar{\boldsymbol{k}} = [\bar{k}_x, 0, \bar{k}_z]$, with an electromagnetic field that obeys Expression (6), where p is m or d, respectively for the metal or dielectric [2], [3], [6], [8].

$$\begin{cases} \bar{E}_{x,p}(x,y,z,t) = E_0 e^{j(\bar{k}_x x + \bar{k}_{z,p}|z| - \omega t)} \\ \bar{E}_{z,p}(x,y,z,t) = \pm\frac{\bar{k}_x}{\bar{k}_{z,p}} E_0 e^{j(\bar{k}_x x + \bar{k}_{z,p}|z| - \omega t)} \\ \bar{H}_{y,p}(x,y,z,t) = H_0 e^{j(\bar{k}_x x + \bar{k}_{z,p}|z| - \omega t)} \end{cases} \tag{6}$$

In the absence of surface free charges, boundary conditions imply that $\bar{E}_{x,d} = \bar{E}_{x,m}$ and $\bar{H}_{y,d} = \bar{H}_{y,m}$. Then, deduction of Expression (7) is valid and consequently it is possible to obtain Expression (8), where k_0 is the incident wavevector, and $\bar{\epsilon}_m$ and $\bar{\epsilon}_d$ are respectively the metal (plasma) and the dielectric relative electric permittivity [2]–[4], [6].

$$\boldsymbol{\nabla} \times \bar{\boldsymbol{H}} = \bar{\epsilon} \frac{\partial \bar{\boldsymbol{E}}}{\partial t} \Rightarrow \begin{cases} \frac{E_0}{H_0} = -\frac{\bar{k}_{z,1} c_0}{\bar{\epsilon}_m \omega} \\ \frac{E_0}{H_0} = \frac{\bar{k}_{z,d} c_0}{\bar{\epsilon}_d \omega} \\ \bar{k}^2 = \bar{k}_x^2 + \bar{k}_z^2 \end{cases} \Rightarrow \begin{cases} \frac{\bar{k}_{z,m}}{\bar{\epsilon}_m} + \frac{\bar{k}_{z,d}}{\bar{\epsilon}_d} = 0 \\ \bar{k}_x^2 + \bar{k}_{z,p}^2 = \bar{\epsilon}_p \left(\frac{\omega}{c_0}\right)^2 \end{cases} \tag{7}$$

$$\bar{k}_x = k_0 \sqrt{\frac{\bar{\epsilon}_m(\omega)\bar{\epsilon}_d(\omega)}{\bar{\epsilon}_m(\omega) + \bar{\epsilon}_d(\omega)}} \tag{8}$$

On the top of that, a perpendicular wavevector component $\bar{k}_z$ appears, such as $\bar{k}_{z,p} = (\bar{\epsilon}_p k_0^2 - \bar{k}_x^2)^{1/2}$.

Some examples of the SPP dispersion relation curves, $\omega(Re\{k_x\})$, are presented below, however it is important to highlight at this point that SPP have a evanescent decay, since its curves are on the right side of the light one ($\omega = c_0 \frac{Re\{k_x\}}{n\sqrt{\bar{\epsilon}_d(\omega)}}$, where c_0 is the vacuum light speed and n is the dielectric refractive index) [1], [3]–[7].

C. Implemented Approach

The proposed methodology is based on the propagation of inhomogeneous light at a dielectric-metal interface. Since the metal medium is a highly absorbing media at optical frequencies (visible and infrared spectral regions), the light wave, ray or particle is defined as inhomogeneous and consequently, the normal direction at the plane of constant phase, $\hat{\boldsymbol{e}}$, and at the plane of constant amplitude, $\hat{\boldsymbol{g}}$, may not be coincident. Also, $\hat{\boldsymbol{e}}$ and $\hat{\boldsymbol{g}}$ are in the same plane of incidence, but they are separated by an angle α such as $cos(\alpha) = \hat{\boldsymbol{e}} \cdot \hat{\boldsymbol{g}}$ [13]–[17].

The complex electrical permittivity of the metal, modelled by the Drude-Lorentz Expression (5), lead to the propagation of inhomogeneous light with a wavevector characterised by Expressions (9) and (10), being $\hat{\boldsymbol{s}}$ a vector perpendicular to the interface. Thus, θ and ψ are the incidence angles of respectively, the real and imaginary wavevectors (representative of a wave, ray or particle). Furthermore, *N* and *K* are the apparent refractive index components, which might be calculated by Expression (11), where n and k are respectively the real and imaginary parts of the complex refractive index. Based on previous expressions it is possible to deduce Expression (12), useful to determine *N* values. On top of that, *K* values must be computed after obtaining the *N* values, using Expression (11) [13]–[17].

$$\bar{\boldsymbol{k}} = k_0 \left(N\hat{\boldsymbol{e}} + jK\hat{\boldsymbol{g}}\right) \tag{9}$$

$$\bar{\boldsymbol{k}} \cdot \hat{\boldsymbol{s}} = \bar{k} = k_0 \left(N\, cos\left(\theta\right) + j\, K\, cos\left(\psi\right)\right) \tag{10}$$

$$\begin{cases} N^2 - K^2 = n^2 - \kappa^2 \\ NK\hat{\boldsymbol{e}} \cdot \hat{\boldsymbol{g}} = n\kappa \end{cases} \tag{11}$$

$$N^2 = \frac{1}{2}\left(n^2 - \kappa^2 + \sqrt{(n^2-\kappa^2)^2 + 4\left(n\kappa/cos\left(\alpha\right)\right)}\right) \tag{12}$$

At the interface, the complex components of $\boldsymbol{k}$ must be conserved, due to boundary conditions. Based on that, the incidence (θ_i and ψ_i) and transmission (θ_t and ψ_t) angles are related by Expression (13). Also, the incidence and reflection angles should be equal, $\theta_r = \theta_i$ and $\psi_r = \psi_i$.

$$\begin{cases} N_i \sin\left(\theta_i\right) = N_t \sin\left(\theta_t\right) \\ K_i \sin\left(\psi_i\right) = K_t \sin\left(\psi_t\right) \end{cases} \tag{13}$$

Considering this approach, it is possible to establish the Fresnel power coefficients of reflection and transmission, presented respectively in Expressions (14) and (15). However, the expression $R + T = 1$ is not valid for absorbing media and two different coefficients should be added, such that $R + T + L = 1 + M$ [13]–[17]. The coefficient L is dependent on the superficial conductivity (due to the surface charges), σ_s, which is neglected in this article, assuming $\sigma \gg \sigma_s$ (σ is the materials' conductivity and it is related to the imaginary part of the complex electrical permittivity). Moreover, this assumption is the same made before when analysing the interface directly based on Maxwell's laws, leading to rigorously the same boundary conditions. However, the effects of this term are related to the power absorption on the surface, increase in reflectivity and decrease in transmission. On the other hand, M is the interference coefficient defined by expression 16 and it is computed using expression 16. This term corrects the transmission coefficient [14]. Thus, the power reflection and transmission percentage are R and $T - M$, respectively [14].

$$R_p = \left|\frac{\bar{n}_t^2\bar{k}_i - \bar{n}_i^2\bar{k}_t}{\bar{n}_t^2\bar{k}_i + \bar{n}_i^2\bar{k}_t}\right|^2 \tag{14}$$

$$T_p = \frac{Re\{\bar{k}_t/\bar{n}_t^2\}}{Re\{\bar{k}_i/\bar{n}_i^2\}}\left|\frac{2\bar{k}_i/\bar{n}_i^2}{\bar{k}_i/\bar{n}_i^2 + \bar{k}_t/\bar{n}_t^2}\right|^2 \tag{15}$$

$$M_p = Im\left\{\frac{\bar{n}_t^2\bar{k}_i - \bar{n}_i^2\bar{k}_t}{\bar{n}_t^2\bar{k}_i + \bar{n}_i^2\bar{k}_t}\right\}\frac{Im\{2\bar{k}_i/\bar{n}_i^2\}}{Re\{\bar{k}_i/\bar{n}_i^2\}} \tag{16}$$

On top of that, based on this approach, it is possible to verify that the power absorption ratio is given by Expression (17), where d is the propagation distance.

$$A = e^{-k_0\tilde{}Kcos(\alpha)d} \tag{17}$$

III. Metal Dispersion Relation

As previously referred, SPP have evanescent decay and consequently, their dispersion relation is on the right side of the line curve.

The real and imaginary part of $k_x = k_{SPP}$ at the air-metal interface are presented in Figs. 2 and 3, for the four metals already characterised by the Drude-Lorentz model.

Denoting ϵ' and ϵ'' as respectively the real and imaginary part of the complex electrical permittivity, and assuming that the dielectric has a real permittivity, it is verified that for $\epsilon'_m > 0$, both x and z components of the wavevector are purely real, leading to radiative modes. However, for $-\epsilon_d < \epsilon'_m < 0$ the imaginary part of $\bar{k}_x$ is much higher than its real part, meaning that there is quasi-bound modes of propagation. Also, for $\epsilon'_m < -\epsilon_d$ the x component of the wavevector is mainly real in contrast with

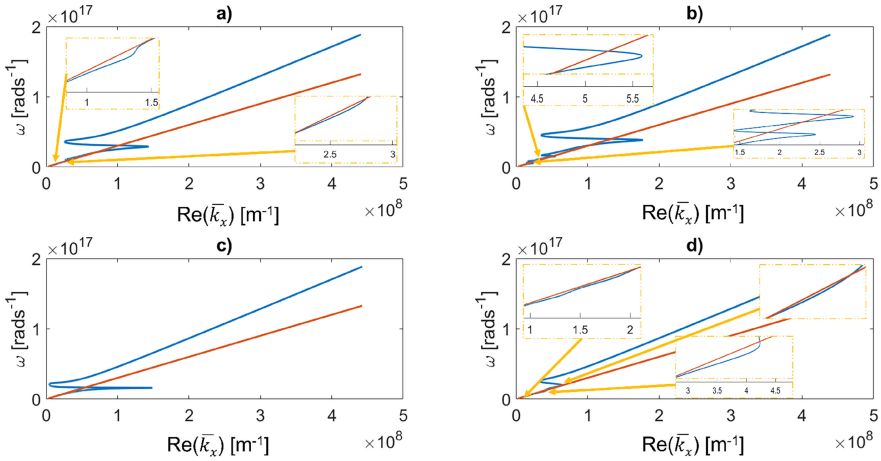

Fig. 2. Wavevector surface component ($\bar{k}_x$) real part of a air-metal interface: a) gold; b) silver; c) aluminium; d) copper. Zoom on SPP frequencies.

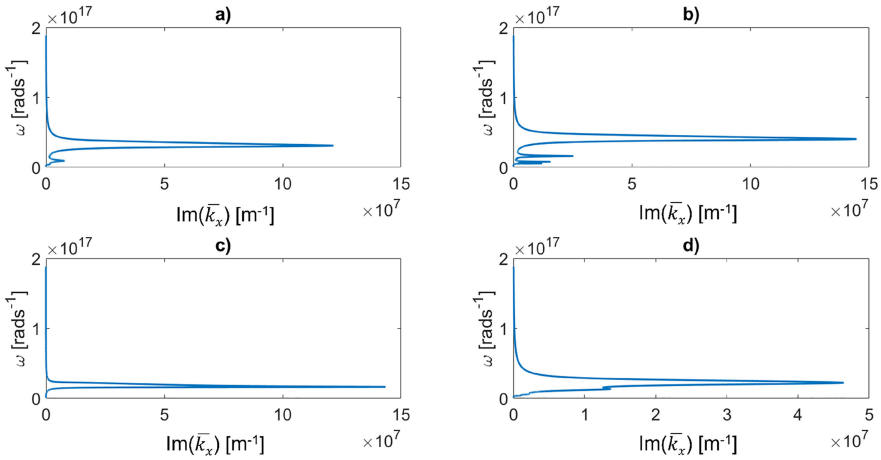

Fig. 3. Wavevector surface component ($\bar{k}_x$) imaginary part of a air-metal interface: a) gold; b) silver; c) aluminium; d) copper.

TABLE II
WAVELENGTHS WITH EXPECTED RESONANCE

Metal	Gold	Silver	Aluminium	Copper
λ	64 nm 238 nm 536 nm	49 nm 123 nm 249 nm 355 nm	118 nm	85 nm 158 nm 360 nm 550 nm

the z component which is mostly imaginary, leading to bound modes [6].

Moreover, the real part of $\bar{k}_x$ tends asymptotically to $\frac{\omega_p}{\sqrt{1+\epsilon_d}}$, as the limit between the quasi-bound and bound modes region (maximum of k_x values on Fig. 2 below the light curve). Radiative mode are on the left side of the light curve for angular frequencies higher than ω_p. Between $\frac{\omega_p}{\sqrt{1+\epsilon_d}}$ and ω_p are the quasi-bound modes as well as below $\frac{\omega_p}{\sqrt{1+\epsilon_d}}$ are the bound ones [6].

Based on Figs. 2 and 3 it is possible to extrapolate the resonance wavelengths for the air-metal interfaces. These resonances wavelengths are presented in Table II. They are calculated analysing those figures, and determining the transition wavelengths for which the imaginary part of $\bar{k_x}$ becomes from much greater to much smaller than its real part.

IV. TRANSMISSION PROBABILITY - TRANSMISSION ANGLE ANALYSIS

The methodology is implemented in Python and in this section, it is analysed the transmission angle θ_t and the transmission percentage of an incident wave by sweeping both incidence angle and wavelength. Since $n_i = N_i = 0 \Rightarrow \Psi_t = 0$, meaning that the waves on the metal are evanescent as predicted. For that reason, charts about Ψ_t are not presented, because they are null. This means that the plane of constant amplitude is parallel to the interface.

The figures of this section should be analysed as maps or charts, since not all the transmission angles are allowed. Only the ones with a non-null transmission probability(particle)/percentage(wave). Furthermore, since an electromagnetic wave might be composed of several rays with different directions (incidence angles), the transmitted wave will also be composed by different transmitted rays, once again with

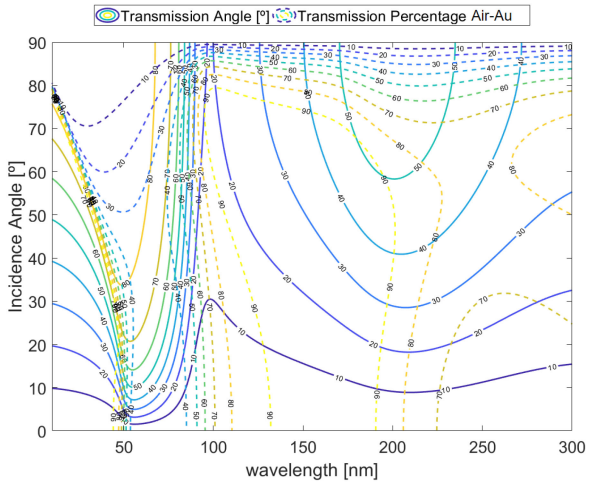

Fig. 4. Transmission angle and transmission percentage/probability in function of the incident wavelength and angle for the air-gold interface on the wavelength range 10-300 nm (SPP resonance near 64 nm and 238 nm).

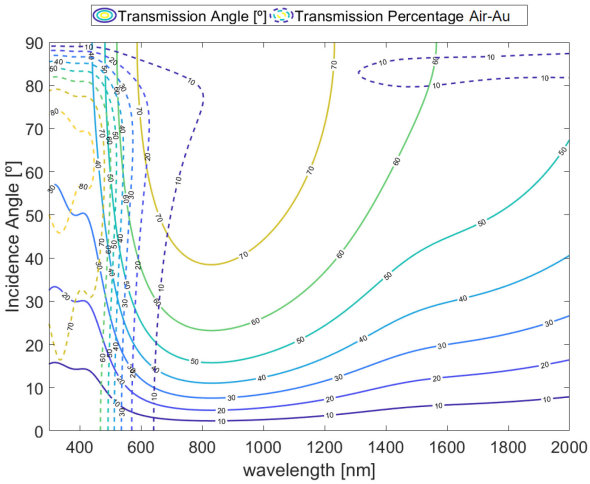

Fig. 5. Transmission angle and transmission percentage/probability in function of the incident wavelength and angle for the air-gold interface on the wavelength range 300-2000 nm (SPP resonance near 536 nm).

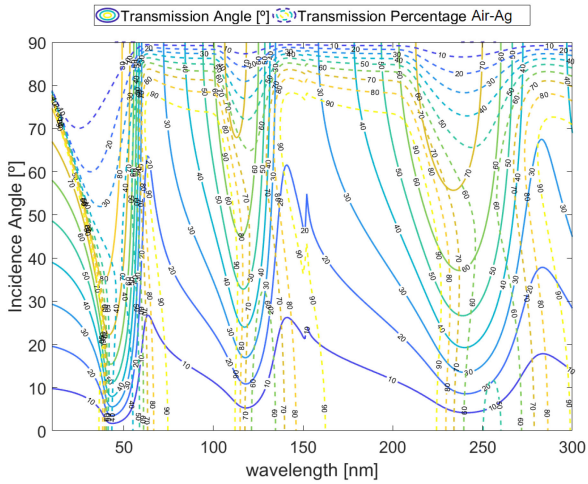

Fig. 6. Transmission angle and transmission percentage/probability in function of the incident wavelength and angle for the air-silver interface on the wavelength range 10-300 nm (SPP resonance near 49 nm, 123 nm and 249 nm).

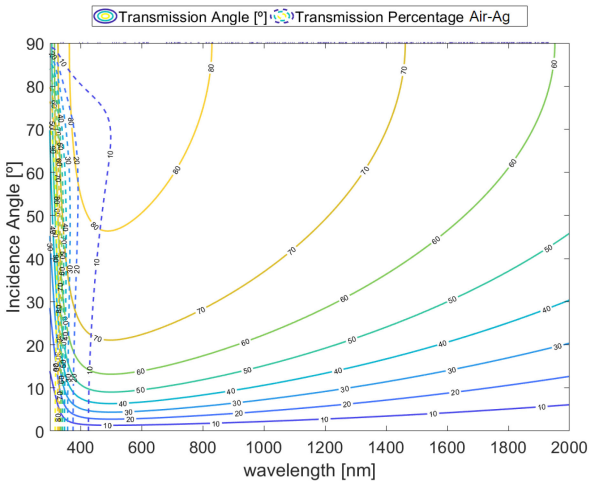

Fig. 7. Transmission angle and transmission percentage/probability in function of the incident wavelength and angle for the air-silver interface on the wavelength range 300-2000 nm (SPP resonance near 355 nm).

different angles. Some of these angles or transmission directions are affected by the SPP phenomenon.

The charts for the air-gold interface are in Figs. 4 and 5. As expected, and presented on previous sections, this interface should have an SPP resonance at 64 nm, 238 nm and 536 nm. Analysing these figures, it is possible to verify that the transmission angle (propagation direction of $\bar{k}_t$) achieves high values. Near these resonance wavelengths, a particular behaviour is obtained, namely there is an abrupt appearance of higher transmission angles. On top of that, it is possible to verify that the transmission percentage is not null, and its value is quite considerable and impressive when compared with its null value on microwaves regimes.

It is also noticeable a different resonance at 97 nm. It is a resonance of the gold electrical permittivity, and the obtained value is quite huge in comparison with the resonance value at the dielectric-metal interface. Thus, small transmission angles dominate in contrast with the ample transmission angles (transmission closer to the surface) obtained on SPP resonance. This is also detectable on the dispersion relation curves, since at this wavelength there is a peak on the imaginary part of $\bar{k}_x$, being its real part practically null.

Silver resonances are near 49 nm, 123 nm, 249 nm and 355 nm as previously predicted. In Figs. 6 and 7 is noticeable that their behaviour is identical to the gold ones. However, since the higher resonance wavelength in the silver predictions is 355 nm and in the gold interface is 536 nm, it is possible to verify on Fig. 7 that in the visible region the silver-air interface has a smaller transmission percentage. In other words, the air-gold interface has transmissions along almost all the visible part of the spectrum in contrast with the air-silver interface.

The aluminium behaviour is different from gold and silver ones. The aluminium's resonance is at 118 nm and it is visible in Fig. 8. However, near 800 nm the imaginary part of $\bar{k}_x$ has a

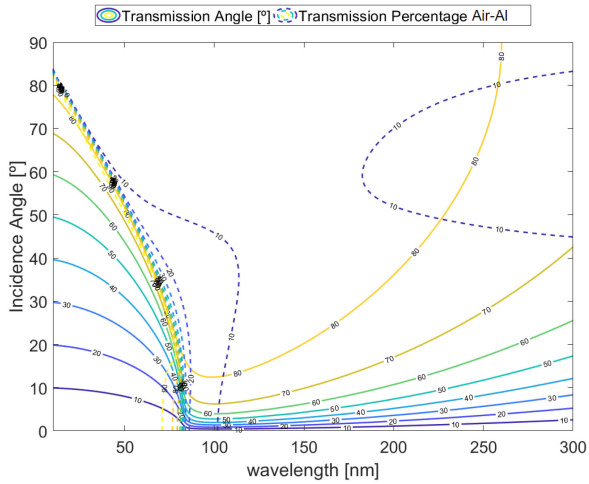

Fig. 8. Transmission angle and transmission percentage/probability in function of the incident wavelength and angle for the air-aluminium interface on the wavelength range 10-300 nm (SPP resonance near 118 nm).

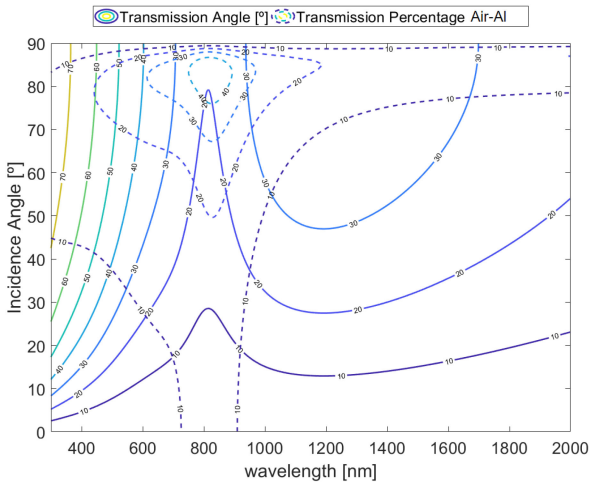

Fig. 9. Transmission angle and transmission percentage/probability in function of the incident wavelength and angle for the air-aluminium interface on the wavelength range 300-2000 nm.

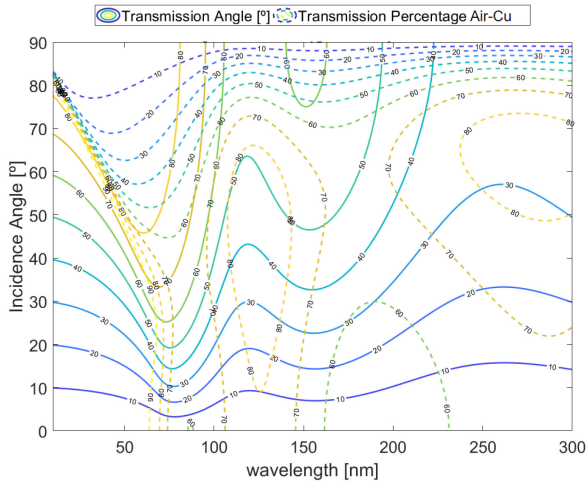

Fig. 10. Transmission angle and transmission percentage/probability in function of the incident wavelength and angle for the air-copper interface on the wavelength range 10-300 nm (SPP resonance near 85 nm and 158 nm).

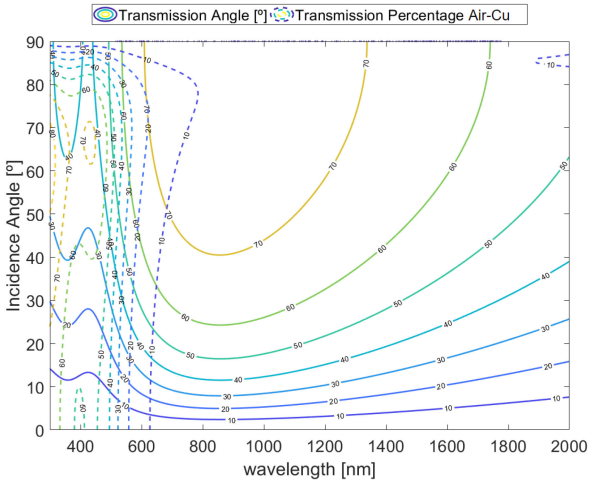

Fig. 11. Transmission angle and transmission percentage/probability in function of the incident wavelength and angle for the air-copper interface on the wavelength range 300-2000 nm (SPP resonance near 360 nm and 550 nm).

small peak that leads to the general increase of the transmission percentage as well as the decrease of transmission angles. This means that the wave is more evanescent and it will decay/be absorbed closer to the interface. The angle $\alpha = \theta - \psi$ tends to zero, leading to the increase in the absorption ratio of Expression (17). This effect will also be observed in the propagation length figures, in the following section.

The last metal is copper, which charts are presented in Figs. 10 and 11. The resonances are near 85 nm, 158 nm, 360 nm and 550 nm as predictable. The importance of analysing a metal as copper is due to the fact that there is a double resonance on the visible spectral region. The cleaner resonance appears on aluminium, since there is mostly one plasma frequency, which is visible in Figs. 2 and 3. Zooming in the copper's dispersion relation it is possible to verify a region where there are two peaks of $\bar{k}_x$. These peaks are so close that there is no room to treat them independently. This means that the visible region is influenced by a superposition of two different resonances. In Fig. 11 is possible to verify this behaviour, where generally the transmission angles increase in this region.

V. Transmission Probability - Propagation Length Analysis

After analysing the transmission percentage and angle, it is also quite interesting to investigate and observe the behaviour of the propagation length.

Propagation length is defined as the distance for which the electromagnetic field decays $1/e$. From the particle point of view, it is the photons' average travelling distance, before being absorbed. This means that the propagation length might be computed using Expression (17), determining the distance d, for which the power absorption is $1/e^2$.

It is already known that this kind of waves has a propagation length in the nanometres range. This is the justification for which phenomena as Extraordinary Optical Transmission (EOT) are only observable at nano structures. The transmitted wave might

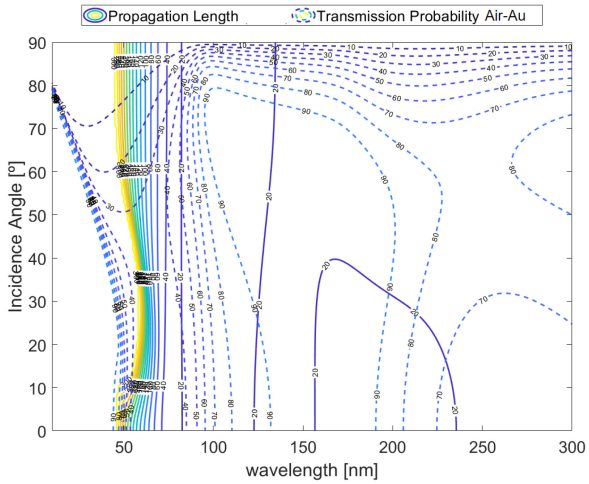

Fig. 12. Propagation length and transmission percentage/probability in function of the incident wavelength and angle for the air-gold interface on the wavelength range 10-300 nm (SPP resonance near 64 nm and 238 nm).

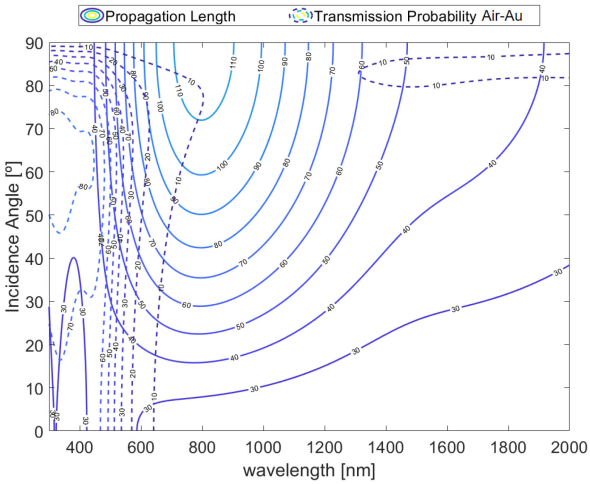

Fig. 13. Propagation length and transmission percentage/probability in function of the incident wavelength and angle for the air-gold interface on the wavelength range 300-2000 nm (SPP resonance near 536 nm).

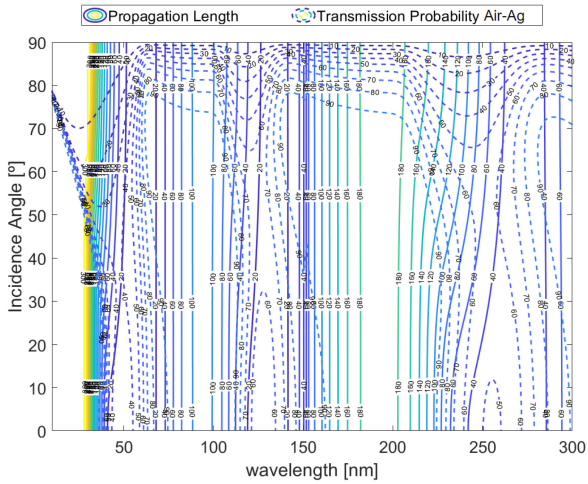

Fig. 14. Propagation length and transmission percentage/probability in function of the incident wavelength and angle for the air-silver interface on the wavelength range 10-300 nm (SPP resonance near 49 nm, 123 nm and 249 nm).

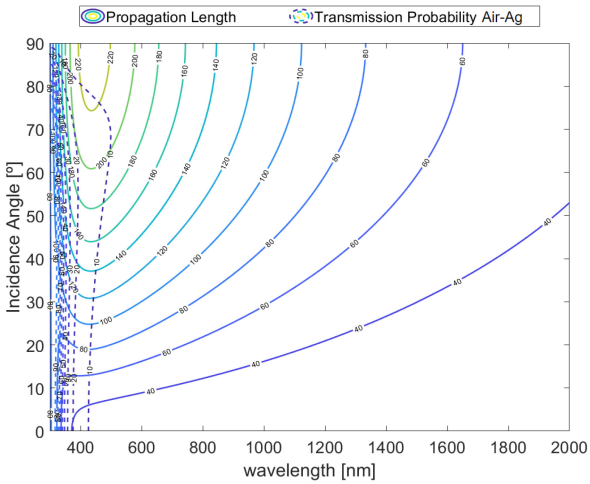

Fig. 15. Propagation length and transmission percentage/probability in function of the incident wavelength and angle for the air-silver interface on the wavelength range 300-2000 nm (SPP resonance near 355 nm).

come out from the metal however, it cannot be absorbed before. For this reason, new nano-scale phenomena appear.

In Figs. 12 and 13 are presented the propagation length in gold. It is possible to corroborate the above paragraph statements. Also, it is observed that the propagation length is dependent not only on the wavelength but also on the incident angle, as predictable from Expression (17). The propagation length on the infrared region might reach more than twice the values in the visible and ultraviolet regions. The near-infrared is the region with higher values, but there is also a smaller wave transmission percentage.

Figs. 14 and 15 presents the propagation length of silver. Comparing these results with gold ones, it is possible to verify that on surface plasma polaritons resonances the behaviour of the propagation length curves is different. First, it is possible to divide these charts into two different regions plus a transition one. Above the resonance frequencies, the propagation length tends to have a linear behaviour with the incident wavelength. It is visible the tendency to horizontal lines, meaning it is almost independent of the incident wavelength. On top of that, for small incident wavelengths it is observed vertical lines, meaning that the propagation length is not dependent on the incident angle. The transition between both regions occurs on the resonances.

The aluminium propagation length results are illustrated in Figs. 16 and 17. These results also confirm the previous analysis. Once again, it is visible that aluminium's response has different properties than the other three noble metals. At 800 nm there is a peak of $\bar{k}_x$ imaginary part, meaning that the propagation length decreases.

As already verified, copper presents a similar behaviour with gold, despite having different resonance frequencies. In the same way, the results in Figs. 18 and 19 allow us to divide them into mainly two different regions. In this case, due to the double resonance, it is possible to verify a different pattern on the propagation length curve, where there is a double curvature near 400 nm.

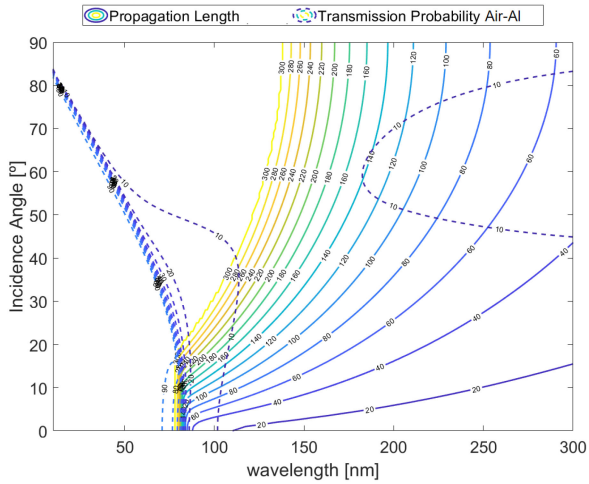

Fig. 16. Propagation length and transmission percentage/probability in function of the incident wavelength and angle for the air-aluminium interface on the wavelength range 10-300 nm (SPP resonance near 118 nm).

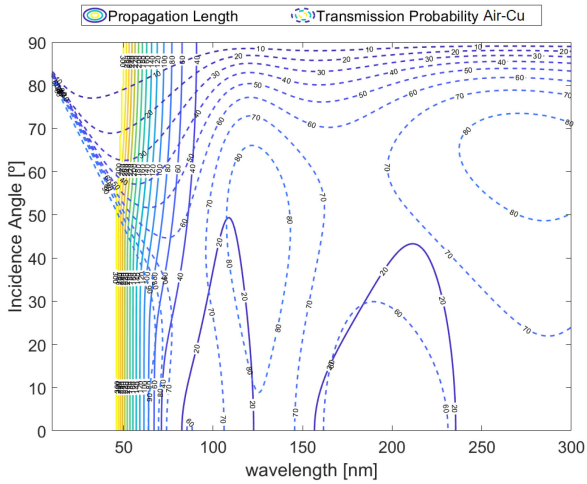

Fig. 18. Propagation length and transmission percentage/probability in function of the incident wavelength and angle for the air-copper interface on the wavelength range 10-300 nm (SPP resonance near 85 nm and 158 nm).

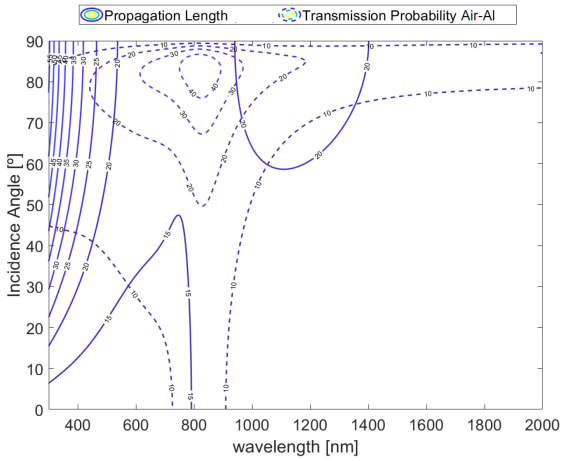

Fig. 17. Propagation length and transmission percentage/probability in function of the incident wavelength and angle for the air-aluminium interface on the wavelength range 300-2000 nm.

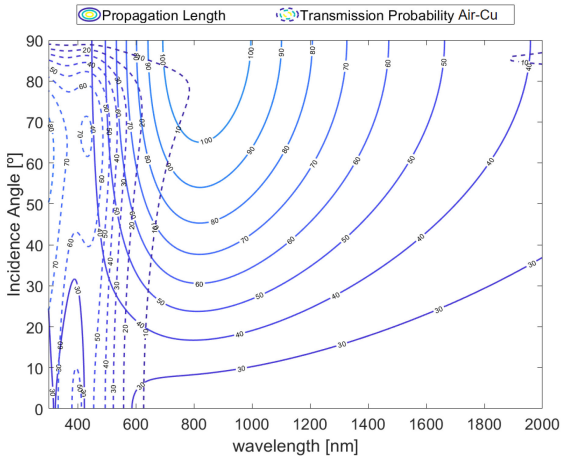

Fig. 19. Propagation length and transmission percentage/probability in function of the incident wavelength and angle for the air-copper interface on the wavelength range 300-2000 nm (SPP resonance near 360 nm and 550 nm).

Thus, it is observed that near resonance wavelengths the propagation length is highly dependent on both incident wavelength and angle. Below it, there is only wavelength influence and above it, there is only angle dependence.

VI. Conclusion

The proposed methodology allows us to have a different perception of what are the phenomena and their implications on dielectric-metal interfaces at optical frequencies. The proposed method allows us to focus more attention on the interface. It is oriented for plane waves. However, at the nano-scale where sources might be near the interfaces, there are no plane waves but a composition of different plane waves at several angles (cylindrical waves).

Based on the obtained results it is possible to point out some important and novel conclusions. First, the transmission percentage has important local maxima and minima near resonance frequencies. However, it is possible to verify that the transmission percentage has impressive high values (in comparison with the null percentage at microwave regimes). Additionally, these non-null probabilities are combined with also high transmission angles, meaning that power must be transmitted closer to the surface. Analysing this fact and the charts behaviour (resonances on the predictable wavelengths) it is possible to conclude that surface plasmon polaritons are the main agents on the transmission peaks in ultraviolet and visible regions. Furthermore, propagation length is analysed, and the results show us this kind of phenomenon is only observable at the nano-scale, since the transmitted waves/particles only propagates orders of 50-100 nm. This is quite relevant since it is not only important to have a subwavelength structure but also to work at optical frequencies. The work on optical frequencies allow the transmission and propagation in the metal. The subwavelength dimensions allow the appearance of these waves/particles at other interfaces, meaning that it is possible to use them before being absorbed and in certain cases, re-transmit them for non or less absorbing media (for instance EOT).

The illustrated charts, obtained using the proposed methodology, allow us to have a better idea about SPP resonances. For instance, it is quite useful when choosing the correct materials for a certain application, since it is possible to verify in which conditions radiation is reflected or transmitted by the interface. Also, the proposed methodology based on the Maxwell's equations, give us a grounded understanding of surface plasmon polaritons role and wave propagation, throughout the interface. This approach is based on optical concepts, such as Fresnel Coefficients and Generalised Snell's law.

REFERENCES

[1] T. W. Ebbesen, H. J. Lezec, H. F. Ghaemi, T. Thio, and P. A. Wolff, "Extraordinary optical transmission through sub-wavelength hole arrays," *Nature*, vol. 391, pp. 667–669, 1998.

[2] J. Zhang, J. B. Pendry, and Y. Luo, "Transformation optics from macroscopic to nanoscale regimes: A review," *Adv. Photon.*, vol. 1, no. 1, 2019, Art. no. 014001.

[3] P. Lalanne and H. Liu, "The elementary interactions in the extraordinary optical transmission phenomenon," *J. Phys. Conf. Ser.*, vol. 139, 2008, Art. no. 012001.

[4] C. Sauvan, C. Billaudeau, S. Collin, N. Bardou, F. Pardo, and J.-L. Pelouard, "Surface plasmon coupling on metallic film perforated by two-dimensional rectangular hole array," *Appl. Phys. Lett*., vol. 92, 2008, Art. no. 011125.

[5] K. Xu, M. Fang, and Z. Huang, "Compact vertical-cavity surface-emitting laser based on all-dielectric metasurfaces," *Opt. Commun.*, vol. 475, 2020, Art. no. 126257.

[6] R. D. F. R. Gomes, M. J. Martins, A. Baptista, and J. P. N. Torres, "Study of a nano optical antenna for intersatellite communications," *Opt. Quant. Electron*, vol. 49, 2017, Art. no. 135.

[7] R. A. M. Lameirinhas, J. P. N. Torres, A. Baptista, and M. J. M. Martins, "The impact of nanoantennas on ring resonators' performance," *Opt. Commun.*, vol. 490, 2021, Art. no 126906.

[8] J. M. Pitarke, V. M. Silkin, E. V. Chulkov, and P. M. Echenique, "Theory of surface plasmons and surface-plasmon polaritons," *Rep. Progress Phys.*, vol. 70, no. 1, 2006, Art. no. 1.

[9] L. Novotny and N. Van Hulst, "Antennas for light," *Nat. Photon.*, vol. 5, no. 2, pp. 83–90, 2011.

[10] N. Sharma *et al.*, "Fuchs Sondheimer–Drude lorentz model and drude model in the study of SPR based optical sensors: A theoretical study," *Opt. Commun.*, vol. 357, pp. 120–126, 2015.

[11] M. N. Polyanskiy, "Refractive index database," Accessed: Sep. 15, 2021. [Online]. Available: https://refractiveindex.info

[12] A. D. Rakić, A. B. Djurišić, J. M. Elazar, and M. L. Majewski, "Optical properties of metallic films for vertical-cavity optoelectronic devices," *Appl. Opt.*, vol. 37, pp. 5271–5283, 1998.

[13] S. Zhang *et al.*, "Generalized laws of snell, fresnel and energy balance for a charged planar interface between lossy media," *J. Quantitative Spectrosc. Radiative Transfer*, vol. 245, 2020, Art. no 106903.

[14] H. Weber, "The fresnel equations for lossy dielectrics and conservation of energy," *J. Modern Opt.*, vol. 61, no. 15, pp. 1219–1224, 2014.

[15] P. C. Y. Chang, J. G. Walker, and K. I. Hopcraft, "Ray tracing in absorbing media," *J. Quantitative Spectrosc. Radiative Transfer*, vol. 96, no. 3/4, pp. 327–341, 2005.

[16] M. A. Dupertuis, M. Proctor, and B. Acklin, "Generalization of complex snell-descartes and fresnel laws," *JOSA A*, vol. 11, no. 3, pp. 1159–1166, 1994.

[17] J. J. Foley *et al.*, "Inhomogeneous surface plasmon polaritons," *ACS Photon.*, vol. 1, pp. 739–745, 2014.